HOKKAIDO UNIVERSITY

Title	Anisotropic velocity distribution of desorbing product in carbon monoxide oxidation on palladium (110)
Author(s)	Matsushima, Tatsuo; Shobatake, Kosuke; Ohno, Yuichi; Tabayashi, Kiyohiko
Citation	The Journal of Chemical Physics --, 97(4), 2783-2789 https://doi.org/10.1063/1.463070
Issue Date	1992-08
Doc URL	http://hdl.handle.net/2115/5516
Rights	Copyright © 1992 American Institute of Physics
Type	article
File Information	JCP97-4.pdf

Instructions for use

Hokkaido University Collection of Scholarly and Academic Papers : HUSCAP

Anisotropic velocity distribution of desorbing product in carbon monoxide oxidation on palladium (110)

Tatsuo Matsushima
Catalysis Research Center, Hokkaido University, Sapporo 060, Japan
Kosuke Shobatake, Yuichi Ohno, and Kiyohiko Tabayashi
Institute for Molecular Science, Myodaiji, Okazaki 444, Japan

(Received 13 January 1992; accepted 8 May 1992)

Significant anisotropy was found in the velocity distributions of desorbing product CO_2 from a Pd(110) surface. The velocity distributions were determined by a cross-correlation time-of-flight technique combined with angle-resolved thermal desorption. Heating the coadlayer of CO and oxygen produces five peaks in the CO_2 formation spectrum; P_1– (around 420 K), P_2– (~370 K), P_3– (~300 K), P_4– (~230 K), and P_5–CO_2 (~170 K). The translational temperature of each CO_2 is much higher than the corresponding surface temperature, and increases in the sequence of P_1– $< P_2$– $< P_3$– $< P_4$– $< P_5$–CO_2. It decreases rapidly with an increase in the desorption angle perpendicular to the surface trough and more slowly parallel to it. This anisotropy is correlated to the reaction site symmetry.

I. INTRODUCTION

In some combinative desorptions, the spatial distribution of the desorption flux of product molecules is sharply collimated along the surface normal.[1] The product is repulsed from the reaction site during the formation in the surface normal direction. The shape of the repulsive potential may be reflected to the spatial and velocity distributions. Here a new reaction dynamics is expected to be able to provide structural information on the reaction site. In fact, the spatial distribution of reactive CO_2 desorption depends on (i) the density of reactants around reaction sites,[2] (ii) the arrangement of surface atoms constituting the sites,[1] and (iii) the orientation.[3,4] However, the spatial distribution is less sensitive to structures, because it is generally determined by the ratio of the normal velocity component to that parallel to the surface plane. The normal component is mainly determined by the repulsive force from the surface.[5] The parallel component is likely to be determined by the surface temperature, since no acceleration is expected in parallel with the surface plane. In fact, the translational temperature reported so far decreases towards the surface temperature with an increase in the desorption angle.[6-9] The above spatial distributions of reactive CO_2 desorption, (i)–(iii), indicate that the parallel component is also modulated by the structure of reaction sites.

This paper reports the velocity distribution of product CO_2 desorbing from a Pd(110) surface. The spatial distribution of reactively desorbed CO_2 from this surface was reported previously.[1] It is sharp in the $[1\bar{1}0]$ direction (along the surface trough), and sharper in the [001] direction (perpendicular to the trough). The velocity has been predicted to decrease more rapidly with an increase in the desorption angle in the [001] direction than in the $[1\bar{1}0]$ direction. This anisotropy in the velocity distribution was actually observed.

The velocity distribution was determined by a cross-correlation time-of-flight (TOF) technique combined with angle-resolved thermal desorption (TDS). This means has several advantages over other methods used for velocity distribution measurements. It can be used for any desorbing molecule, over a wide range of coverages and at low temperatures. Modulated molecular beams are frequently used as a gas source to the surface. The beams are usually modulated by a mechanical chopper, and the arrival time of desorbing products at a detector is measured to get TOF spectra. In CO oxidation on noble metals, however, this method can be applied only at high surface temperatures, since a significant amount of CO_2 is produced at steady state only above 500 K.[8,9] Below this temperature, the surface is eventually covered by CO and the reaction is mostly retarded. A stable desorption flux of hydrogen is obtained by the permeation through a sample crystal by applying a sample gas at a significantly high pressure from the back side. This method is suitable for TOF measurements, since the desorption is continuous without an increase in the background level due to other gases in a measurement chamber and the flux is stable. However, it can be used only for hydrogen and at high surface temperatures.[5-7] Short desorption pulses of surface species can be induced with a high power irradiation from a laser. It provides a short gate time suitable for TOF measurements (Laser-induced thermal desorption spectroscopy; LITDS). However, an extremely high heating rate obscures the velocity distribution of desired species in a definite range of surface temperature.[10] Doppler shifts in the absorption frequency also provide velocity information when a laser light strikes desorbing molecules. The velocity distribution in this method, however, cannot be determined without knowledge of the spatial distributions.[11] Further, types of desorbing molecules detectable are limited.

II. EXPERIMENTAL METHOD

The apparatus consists of a reaction chamber, a chopper chamber, and an analyzer chamber. A top view of the appa-

 0021-9606/92/162783-07$06.00 © 1992 American Institute of Physics

ratus is schematically shown in Fig. 1. The reaction chamber has low energy electron diffraction (LEED)-Auger electron spectroscopy (AES) optics (Perkin–Elmer 15-120), an Ar^+ gun (ULVAC-PHI USG-3), a quadrupole mass spectrometer (ANELVA AGA100), a Bayard–Alpert ionization gage, and a gas-handling system. It is pumped out by an ion pump of 320 ℓ/s. A sample crystal is set on the bottom top of an L-shaped manipulator. It can be rotated at the top to change the desorption angle (polar angle; θ).

The chopper chamber is pumped out with an ion pump of 160 ℓ/s, a cryopump (Iwatani Model S-30), and a turbomolecular pump (Balzers TPU330). The turbopump was used for an initial evacuation and also for evacuation during baking out of the whole apparatus. During the baking, three chambers were connected together by opening metal valves between each chamber. This procedure was necessary to keep high vacuum conditions, in order to avoid the contamination of a secondary electron multiplier of a mass spectrometer (ULVAC MSQ400) in the analyzer chamber. The chopper disk is made so that slots of equal width (1 mm$\times$6 mm) are distributed in a pseudorandom sequence (with a double sequence of 255 elements each[12]). Time resolution of 15 μs is obtained at a rotation rate of 130.72 Hz. The arrival times at the ionizer (10 mm diameter $\times$ 6 mm height) of the mass spectrometer in the analyzer chamber are registered on a homemade multichannel analyzer running synchronously with the chopper blade. The TOF signal for the temperature range of each CO_2 peak was stored separately. The signal acquisition is controlled by a microcomputer (NEC 9801RA) monitoring the output of a chromel-alumel thermocouple spot welded on the back of the crystal. TOF distributions are obtained after deconvoluting the raw-TOF spectra by using a standard cross-correlation deconvolution technique.[12]

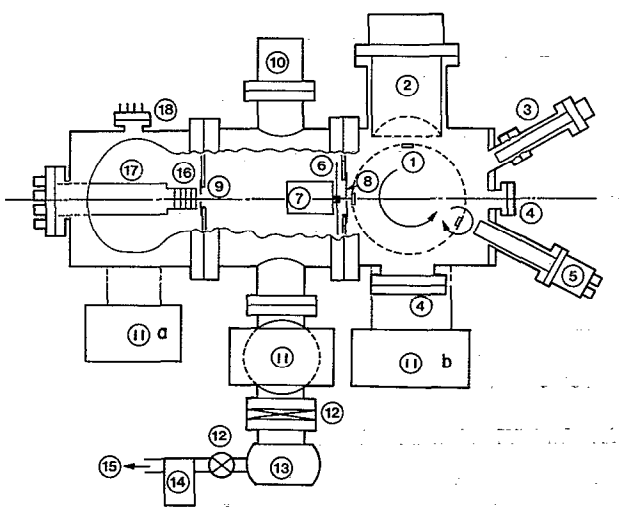

FIG. 1. A top view of the time-of-flight spectrometer combined with angle-resolved thermal desorption. (1) sample crystal, (2) LEED-AES optics, (3) quadrupole mass spectrometer, (4) window, (5) argon ion gun, (6) pseudorandom chopper and photocell for trigger, (7) motor, (8) first slit, (9) second slit, (10) cryopump, (11) ion pump (a and b are beneath the chambers), (12) gate valve, (13) turbomolecular pump, (14) oil diffusion pump, (15) rough pump, (16) ionizer, (17) quadrupole mass spectrometer with a channeltron, (18) BA gage.

A palladium single crystal is a disk-shaped slice (10 mm diameter $\times$ 0.8 mm thickness). It was cut from a rod supplied by Metal Crystal, U.K. Both faces were polished with standard metallographic techniques down to the submicron level. The sample was mounted on the holder by spot welding it to the Ta wires used to heat the crystal. It was cleaned by prolonged Ar^+ bombardment in the temperature range of 300 to 1200 K, and heated in 1×10^{-8} Torr oxygen around 800 K. Finally, the crystal was flashed *in vacuo* up to 1300 K. No impurity was detected with AES at this stage. However, AES is insensitive to carbon on Pd, since the signal is overlapped with that of the substrate itself. Therefore, the sample was further exposed to oxygen at room temperature and heated to remove trace surface carbon as CO. This procedure was repeated until no further CO was found. The LEED pattern showed a sharp (1$\times$1) structure at this stage.

In angle-resolved thermal desorption experiments, the clean and well-ordered Pd(110) surface was exposed to $^{18}O_2$ and $C^{16}O$ sequentially at low temperatures. The surface was resistively heated at a constant rate of 11–15 K/s, while the signal of product $^{12}C^{16}O^{18}O$ was monitored in angle-integrated form by the mass spectrometer in the reaction chamber, and also in angle-resolved form by the other mass spectrometer in the analyzer chamber. In this case, the chopper blade was stopped at the position where an opened slot was in front of the first slit.

For TOF measurements, the flux of $^{12}C^{16}O^{18}O$ passing the first slit (S1:1 mm$\times$6 mm) is modulated by the pseudorandom chopper. The signal is detected after passing the second slit (S2: diameter 5 mm). Thermal desorption procedures were repeated 150–500 times to get a tolerable TOF spectrum. The flight path between the chopper blade and the ionizer measures 304 mm. The distance between S1 and S2 is 299 mm. The sample surface is about 25 mm far from the first slit. The acceptance angle of the aperture of the ionizer is 2.1°$\times$1.1°. The coverages of CO and oxygen, θ_{CO} and θ_O, were determined by thermal desorption and normalized in the way reported previously.[1] The CO coverage on oxygen-covered surfaces is determined in a similar way, since the adsorption of CO is not retarded by preadsorbed oxygen. The usage of $^{18}O_2$ improved the signal-to-noise ratio of the mass spectrometer in the analyzer chamber. ^{18}O will simply be referred to as O in the following, since only $^{12}C^{16}O^{18}O$ is produced in the course of the above procedures.

III. RESULTS

A. General features

The adsorption of CO and oxygen on the present surface was previously reported, as well as the coadsorption.[1] The CO_2 formation during heating of the coadsorption layer yields five peaks in a TDS curve in the range of 150–460 K. In the present experiments, the adsorption of oxygen and CO was carried out sequentially in the range of 230–200 and 190–140 K during cooling of the sample after flashing up to 1300 K. These adsorption procedures yielded a separation of

each CO_2 formation peak better than that at adsorption below 140 K[1]. A series of typical CO_2 formation spectra in angle-integrated form is summarized in Fig. 2(a). With increasing CO exposures, the formation extends to lower temperatures, yielding P_1– around 430 K, P_2– (~320 K), P_3– (~310 K), P_4– (~230 K), and P_5–CO_2 (~170 K). P_2–CO_2 was first observed for high initial oxygen coverages as shown in the figure.[1] The right panel summarizes the angle-resolved spectra observed simultaneously in the surface normal direction ($\theta = 0°$). The signal of P_4–CO_2 and P_5–CO_2 was enhanced in this direction. The comparison of the signals in both forms shows that the angular distribution becomes sharper as the coverage increases.[1]

B. Angular distribution

Typical angle-resolved CO_2 desorption spectra observed at various desorption angles are reproduced in Fig. 3(b). The desorption angle was varied in the [001] direction (perpendicular to the surface trough; the azimuth, $\phi = 0°$). The P_4– and P_5–CO_2 signals enhanced in the normal direction decrease more rapidly with an increase in the desorption angle than the others. The desorption of these CO_2 is more sharply collimated along the surface normal. The desorption of all CO_2 shows angular distributions sharper than a cosine form, as summarized in Table I. The distribution is represented by a power series of cos θ. The power d increases in the sequence of P_1– $< P_2$– $< P_3$– $< P_4$– $< P_5$–CO_2. The distribution of P_4– or P_5–CO_2 is well described by a single power function of cos θ. The results of P_4–CO_2, when the desorption angle is varied in the [1$\bar{1}$0] direction, are shown in Fig. 4.

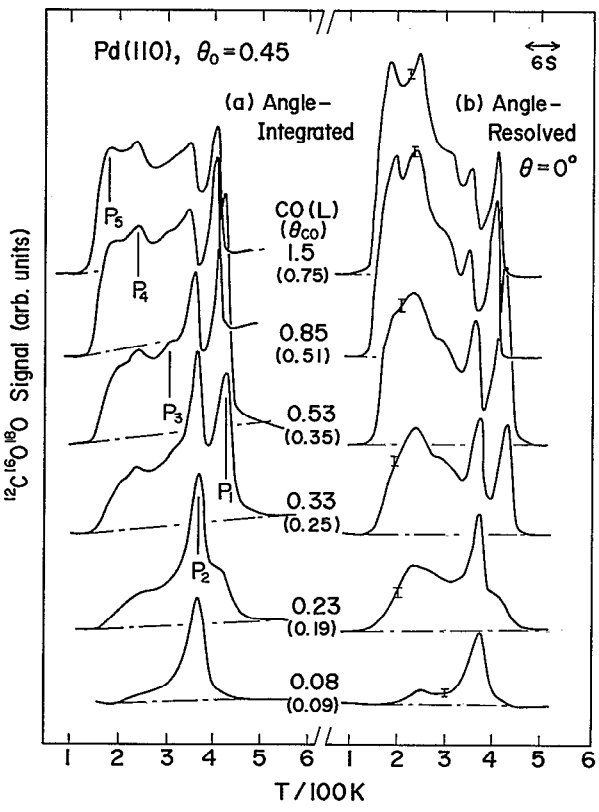

FIG. 2. Typical CO_2 formation spectra generated at a fixed oxygen coverage and various CO exposures in (a) angle-integrated and (b) angle-resolved form in the normal direction. The vertical bars in (b) indicate the noise level. The values in parentheses represent the CO coverage.

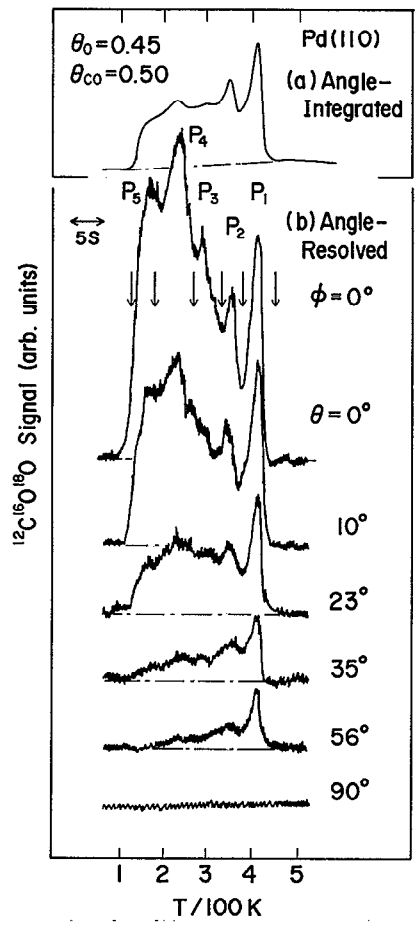

FIG. 3. (a) CO_2 formation spectrum in angle-integrated form at a high CO coverage. The surface precovered with oxygen at $\theta_O = 0.45$ was exposed to 0.80 L (1 Langmuir = 1×10^{-6} Torr s) CO ($\theta_{CO} = 0.50$). (b) Angle-resolved spectra observed at various desorption angles in the [001] direction. The downward arrows indicate the temperatures where the signal accumulation was switched into another channel. The heating rate was 15 K/s.

On the other hand, P_1– and P_2–CO_2 show different behavior. The signal does not follow a single power function. The results of P_1–CO_2 are shown in Fig. 5, where the angle was varied in the [001] direction. The signals at $30° > \theta > -30°$ are well represented by (cos θ).[10] The signals outside this range, however, shift above the curve of this power function. The desorption seems to consist of two components, as described in the discussion section. The desorption of P_2–CO_2 shows a similar behavior with the angle in the [001] direction, although the shift above $\theta = 30°$ is not significant.

The angular distribution of each CO_2 in the [1$\bar{1}$0] direction (along the surface trough) is broader than that in the

TABLE I. Dynamic parameters of desorbing product CO_2 from Pd(110). (A) The desorption angle was varied in the [001] direction. Experimental conditions are shown in Fig. 3. (B) The desorption angle was varied in the [1$\bar{1}$0] direction. The desorption was started from $\theta_O = 0.45$ and $\theta_{CO} = 0.43$.

A	Peak temp.	Angular distr.		Translational temp. $\langle E\rangle/2k$ (K)		
CO_2	(K)	$(\cos\theta)^d$	θ(deg) = 0	17	30	50
P_1	420	$d = 10 \pm 2$	1700 ± 200	1300	900	700[a]
P_2	350	10 ± 2	1700	1450	1200	···
P_3	290	15 ± 3	1900	1700	1300	···
P_4	230	20 ± 4	2100	2050	1800	···
P_5	170	25 ± 5	2300	2200	···	···

B	Angular distr.		Translational temp. $\langle E\rangle/2k$ (K)		
CO_2	$(\cos\theta)^d$	θ(deg) = 0	30	52	67
P_1	$d = 3.0 \pm 0.5$	1600 ± 200	1400	1200	1100
P_2	4.0 ± 0.5	1850	1600	1300	1200
P_3	$6 \sim 10$	2000	1650	1400	···
P_4[b]	15 ± 2	2100	1800	···	···
P_5[b]	20 ± 5	2550	···	···	···

[a] The desorption was initiated at $\theta_O = 0.2$ and $\theta_{CO} = 0.18$.
[b] The desorption was started from $\theta_O = 0.45$ and $\theta_{CO} = 0.62$.

[001] direction, as summarized in Table I(b). The desorption of P_1– and P_2–CO_2 show broad distributions, which are still sharper than a simple cosine form. No indication was found to show two components in the desorption distribution of P_1– or P_2–CO_2 in the [1$\bar{1}$0] direction. The anisotropy in the angular distribution agrees well with the previous results.[1]

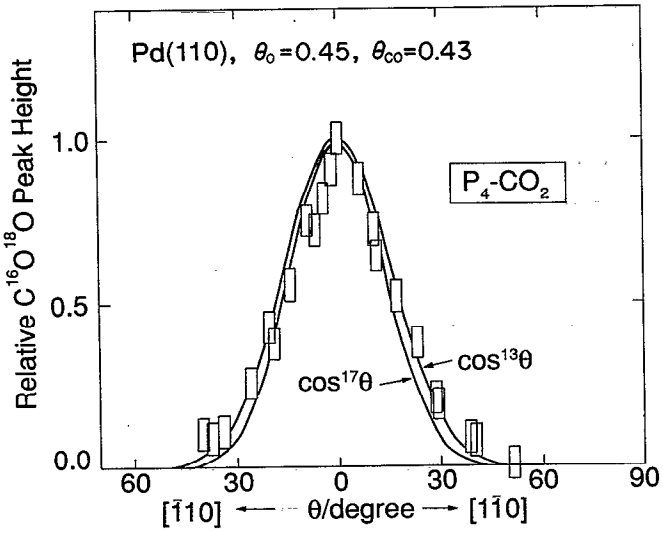

FIG. 4. Angular distribution of the P_4–CO_2 desorption in the [1$\bar{1}$0] direction. The solid lines were drawn for comparison. The initial coverages are given in the figure.

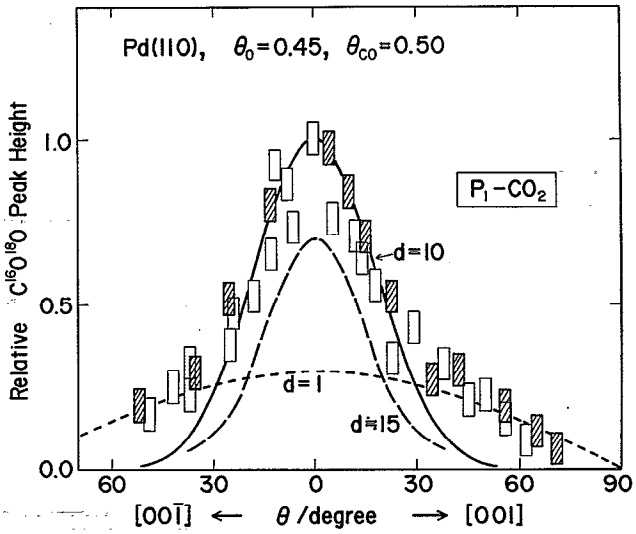

FIG. 5. Angular distribution of the P_1–CO_2 desorption in the [001] direction. The experiment conditions are shown in Fig. 3. Two series of measurements are summarized. The dotted (cosine form) and broken ($\cos^{15}\theta$ dependence) lines represent a typical deconvolution.

C. Velocity distribution

The signal in TOF measurements was accumulated separately for each CO_2 peak. Two channels of the multichannel analyzer were alternatively used in the following temperature ranges: 130–180 K for P_5–CO_2, 180–270 K for P_4–CO_2, 270–325 K for P_3–CO_2, 325–383 K for P_2–CO_2, and 383–450 K for P_1–CO_2. The downward arrows in Fig. 3 indicate these temperatures. A typical TOF spectrum of P_4–CO_2 desorbed in the normal direction is shown in Fig. 6. Thermal desorption was repeated 160 times to obtain this spectrum. The origin of the abscissa shifted due to the ion drift time of the mass spectrometer, $t_{id} = 40\,\mu$s, which was experimentally determined. The maximum signal intensity appears at 220

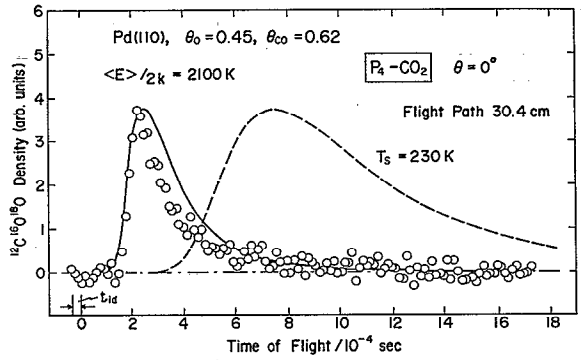

FIG. 6. Typical time-of-flight spectrum of P_4–CO_2 desorbed in the normal direction. $\langle E\rangle/2k = 2100 \pm 200$ K is the estimated translational temperature. The desorption procedure was started at $\theta_O = 0.45$ and $\theta_{CO} = 0.62$. The gate time of the chopper was 15 μs. t_{id} is the ion drift time of $C^{16}O^{18}O$ in the mass spectrometer, 40 μs. The broken line shows a Maxwellian distribution at the peak temperature of P_4–CO_2 formation, and the solid that at the estimated translational temperature.

μs, which yields a velocity of approximately 1.4×10^5 cm/s. The translational temperature was estimated to be 2100 ± 200 K by dividing the mean translational energy, $\langle E\rangle$, by $2k$ (Boltzmann constant).[5] The temperatures of the other CO_2 determined in this way are summarized in Table I. The translational temperature increases with the coverages, i.e., in the sequence of $P_1- < P_2- < P_3- < P_4- < P_5$–$CO_2$. It decreases more rapidly with an increase in the desorption angle in the [001] direction than in the [1$\bar{1}$0] direction.

In order to show a clear decrease of the translational temperature with an increase in the desorption angle, Fig. 7 summarizes typical TOF spectra of P_1–CO_2 observed at various desorption angles in the [001] direction. The position of the maximum intensity shifts toward longer arrival times with the desorption angle. Each solid line represents a Maxwellian distribution at the estimated translational temperature. The signal seems to show another maximum around 550 μs. This sign becomes clear at $\theta = 50°$. This is probably due to a contribution of CO_2 thermalized on the surface before the desorption.

IV. DISCUSSION

A. Coverage dependence

An excess translational energy of desorbing products has been found in some combinative desorptions, which yield sharp angular distributions of the desorption flux.[5–9] This was actually confirmed in the present experiments. A Maxwellian distribution at the peak temperature of P_4–CO_2 formation (230 K) was drawn by the broken line in Fig. 6. It shows the maximum signal intensity at 746 μs. Most of the actual signals appear in the arrival time range much shorter than this distribution. The estimated translational temperature, 2100 ± 200 K, is much higher than the peak temperature. The solid line was calculated by assuming a Maxwellian distribution at the estimated translational temperature. The peak in the TOF curve observed was slightly narrower than this calculated distribution. The observed signal level after the peak time goes below the calculated line. The normalized speed ratio has frequently been used to represent a shift in the velocity distribution from a Maxwellian form. It is defined as $(\langle v^2\rangle/\langle v\rangle^2-1)^{1/2}/(32/9\pi-1),^{1/2}$ where $\langle v^2\rangle$ is the mean square velocity and $\langle v\rangle$ the mean velocity. The value for the TOF spectrum in Fig. 6 was estimated to be 0.87 ± 0.08. This is quite similar to the velocity distribution of hydrogen molecules desorbing through a combinative process of hydrogen adatoms on Ni(111) surfaces.[7] This narrow distribution is caused by the reactive desorption surmounting a high activation barrier extended along the surface normal.[13]

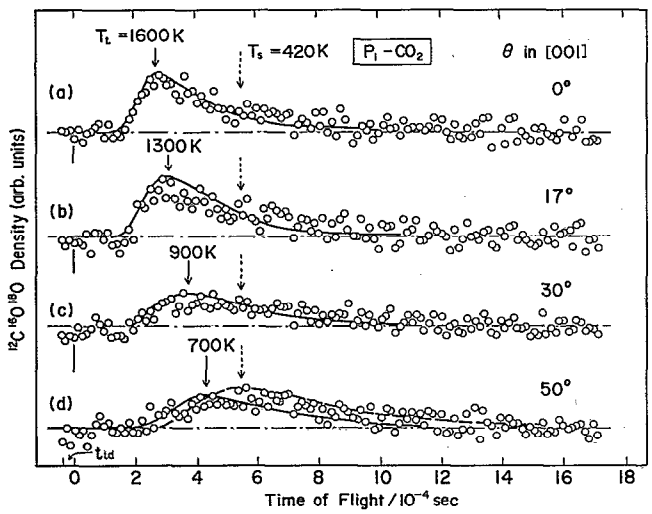

FIG. 7. Time-of-flight spectra of P_1–CO_2 observed at various desorption angles in the [001] direction. The desorption was started at $\theta_O = 0.45$ and $\theta_{CO} = 0.50$ for (a) and (b), and at $\theta_O = 0.20$ and $\theta_{CO} = 0.18$ for (c) and (d). Each solid line shows a Maxwellian distribution at the estimated translational temperature. The downward arrows indicate the peak position of the distribution. The broken line at $\theta = 50°$ was drawn by assuming a Maxwellian distribution at 420 K (the P_1–CO_2 peak temperature). Thermal desorption was repeated (a) 220, (b) 300, (c) 500, and (d) 500 times. The ordinate of each spectrum is represented in arbitrary units.

Now we discuss on the factors contributing to sharp angular distributions at high reactant coverages. The angular distribution becomes sharper as the reactant coverages increase: $P_1- < P_2- < P_3- < P_4- < P_5$–$CO_2$. Their translational temperatures also increase in this sequence. This is the first observation on the coverage dependence of the translational temperature. The TOF experiments reported so far are limited to those at high temperatures (i.e., small coverages), because modulated molecular beams[8,9] or permeation methods[6,7] have been used. In the angle-resolved reactive CO_2 desorption experiments reported so far,[1,2,14,15] the angular distribution becomes always sharper as the density of reactants increases. Therefore, this is a common phenomenon in the CO oxidation. Three factors may contribute to this sharpening. The first is the surface temperature effect. The CO_2 showing sharper angular distributions is formed at lower temperatures (i.e., high coverages). As described in Sec. I, the angular distribution is generally determined by the ratio of the normal velocity component to that parallel to the surface plane. The parallel component, which is mostly controlled by the surface temperature, decreases with decreasing the temperature. The normal component is expected to be insensitive to the surface temperature as predicted by activation barrier models.[16,17] This would lead to a sharp angular distribution at lower temperatures. Experimentally, however, the angular distribution for reactive desorption of H_2 and CO_2 has been reported to be insensitive to the surface temperature.[9,18,19] Hence, this may be a minor effect, if any. In fact, the translational temperature was observed to be higher at lower temperatures (i.e., higher coverages). Here a new model, in which the desorption is accelerated at high coverages, should be proposed.

The second factor is suitable for this model, because it is caused by the repulsive force between adsorbates. The coadsorption structure of CO and oxygen adatoms has been analyzed on Pd(111)[2,20] and Pd(100),[21,22] and also on Pd(110) to some extent.[1] The coadsorption is characteristic of the separate domains of each species. This is caused by a significant repulsive force operative between CO and oxygen. The repulsion gives rise to a high activation energy for the CO_2

formation. The oxygen domain is first compressed into lattices with higher densities, when the oxygen-covered surface is exposed to CO above critical coverages.[2,22] This structure change starts first in local parts of the surface, where the activation energy for the CO_2 formation is reduced by the decrease of the heat of adsorption of reactants. This causes additional CO_2 formation peaks at lower temperatures, when the surface is heated. Such compression may occur in CO domains as well.[22] Mixed coadsorption layers are formed at high CO exposures. The layers are highly reactive, producing CO_2 at lower temperatures. This is the mechanism that yields several CO_2 formation peaks in thermal desorption. Repulsive forces will be exerted upon the CO_2 molecule being produced from surrounding adsorbates as well as the surface itself. The force is increased at higher coverages. This will be able to accelerate the desorption of the product, mostly in the surface normal direction, yielding sharp angular distributions and high excess translational energy, as actually observed.

The third factor, named a *collimation effect* by adsorbates, contributes to sharpening angular distribution, and does not increase velocity. The surface parallel motion of molecules being produced is restricted by adsorbates closely surrounding the reaction site. This may collimate the desorption along the surface normal. This effect is not separated from the second factor, since the relation between the angular distribution and the velocity distribution has not quantitatively been analyzed on the present surface. The contribution of similar effect by substrate atoms is discussed in the next section.

B. Anisotropy in velocity

Strong anisotropy was previously reported in the angular distribution on the surface under discussion.[1] This was confirmed in the new apparatus. Clear anisotropy in the angular distribution of desorption flux has frequently been reported in electron stimulated desorption-ion angular distribution (ESDIAD) experiments. This is caused by the shape of the hindered translation potential well of admolecules immediately before the desorption.[23–25] We have proposed a similar desorption model yielding anisotropic angular distributions; CO_2 is reactively desorbed from an oxygen adsorption site which is located on a long-bridge site in the surface trough. P_1–CO_2 is formed below $\theta_{CO} + \theta_O = 0.3$.[1] The interaction between P_1–CO_2 being produced and the surrounding adsorbates may be ignored. The motion of the product is mostly affected by surface palladium atoms. The trough around oxygen on a long-bridge site is steep in the [001] direction, and fairly flat in the [1$\bar{1}$0] direction because the space is open along the trough. The hindered translational momentum of CO_2 being desorbed, which is converted into the parallel velocity component, is distributed more widely in the [1$\bar{1}$0] direction than in the [001] direction. The resultant velocity component in the [001] direction is expected to be distributed at values smaller than those in the [1$\bar{1}$0] direction. The velocity observed actually will involve more contribution from the parallel component at large desorption angles. This means that the velocity should decrease more rapidly with an increase in the desorption angle in the [001] direction than in the [1$\bar{1}$0] direction. This was actually observed in the present experiments. With increasing coverages, the reaction site is closely surrounded by nonreacting adspecies, yielding sharp angular distributions in both directions. Hence, the anisotropy in CO_2 produced at high coverages becomes less compared with that of P_1–CO_2.

The desorption of P_1–CO_2 shown in Fig. 5 suggests a contribution of a broad angular distribution component. It becomes noticeable at large desorption angles, because the main component has a sharp angular distribution. The presence of the broad component is also suggested in the velocity distribution at $\theta = 50°$ in the [001] direction, as shown in Fig. 7(d). The distribution indicates the presence of a slow CO_2 component, which shows probably the surface temperature. A simple cosine distribution is expected for the angular dependence of the desorption flux and a Maxwellian distribution at the surface temperature for the velocity, if the CO_2 is trapped in the physical adsorption state before the desorption.[26,27] The cosine distribution represented by the dotted curve in Fig. 5 was drawn so as to hit the data above $\theta = 30°$. The dashed curve is the difference between the cosine form and the actual data. It is close to a $(\cos\theta)^{15}$ dependence. This deconvolution, however, does not necessarily mean that two desorption channels are operative. No physical meaning has been found in describing the angular distribution by means of a single power function of $\cos\theta$.

ACKNOWLEDGMENTS

We are indebted to members of the Equipment Development Center, Institute for Molecular Science, for their skillful technical assistance. This work is partly supported by a Grant-in-Aid for General Scientific Research from the Ministry of Education, No. 03640419.

[1] T. Matsushima, J. Chem. Phys. **91**, 5722 (1989), and references therein.
[2] T. Matsushima and H. Asada, J. Chem. Phys. **85**, 1658 (1986).
[3] T. Matsushima, J. Chem. Phys. **93**, 1464 (1990).
[4] T. Matsushima, Y. Ohno, and K. Nagai, J. Chem. Phys. **94**, 704 (1991).
[5] G. Comsa and R. David, Surf. Sci. Rep. **5**, 145 (1985).
[6] M. Balooch and R. E. Stickney, Surf. Sci. **44**, 310 (1974); A. E. Dabiri, T. J. Lee, and R. E. Stickney, *ibid.* **26**, 522 (1971).
[7] G. Comsa, R. David, and B. J. Schumacher, Surf. Sci. **85**, 45 (1979).
[8] C. A. Becker, J. P. Cowin, L. Wharton, and D. J. Auerbach, J. Chem. Phys. **69**, 3394 (1977).
[9] L. S. Brown and S. J. Sibener, J. Chem. Phys. **90**, 2807 (1989).
[10] K. Witan, D. Borgmann, and G. Wedler, Appl. Phys. A **51**, 132 (1990).
[11] R. R. Cavanagh and D. S. King, in *Chemistry and Physics of Solid Surfaces, V*, edited by R. Vanselow and R. Howe (Springer, Berlin, 1984), p. 141; D. S. King and R. R. Cavanagh, in *Chemistry and Structure at Interfaces*, edited by R. B. Hall and A. B. Ellis (VCH, Florida, 1986), p. 25.
[12] G. Comsa, R. David, and B. J. Schumacher, Rev. Sci. Instrum. **52**, 789 (1981).
[13] Y. Ohno, T. Toya, S. Ishi, and K. Nagai, Appl. Surf. Sci. **33/34**, 238 (1988); Y. Ohno, T. Nakamura, and H. Kita, Appl. Phys. A **50**, 551 (1990); **51**, 35 (1990).
[14] T. Matsushima, T. Matsui, and M. Hashimoto, J. Chem. Phys. **81**, 5151 (1984).
[15] Y. Ohno and T. Matsushima, Surf. Sci. **239**, L521 (1990).
[16] W. Van Willigen, Phys. Lett. A **28**, 80 (1968).

[17]G. Comsa, R. David, and K. D. Rendulic, Phys. Rev. Lett. **38**, 775 (1977).
[18]L. K. Verheij, M. B. Hugenschmidt, A. B. Anton, B. Poelsema, and G. Comsa, Surf. Sci. **210**, 1 (1989).
[19]C. T. Rettner, H. A. Michelsen, D. J. Auerbach, and C. B. Mullins, J. Chem. Phys. **94**, 7499 (1991).
[20]H. Conrad, G. Ertl, and J. Küppers, Surf. Sci. **76**, 323 (1978).
[21]E. M. Stuve, R. J. Madix, and C. R. Brundle, Surf. Sci. **146**, 155 (1984).
[22]Y. Ohno, T. Matsushima, K. Shobatake, and H. Nozoye, Surf. Sci. (in press, 1992).
[23]T. E. Madey, J. T. Yates, Jr., A. M. Bradshaw, and F. M. Hoffmann, Surf. Sci. **89**, 370 (1979).
[24]M. Kiskinova, A. Szabo, and J. T. Yates, Jr., Surf. Sci. **205**, 215 (1988).
[25]M. A. Henderson, A. Szabo, and J. T. Yates, Jr., J. Chem. Phys. **91**, 7255 (1989); Chem. Phys. Lett. **168**, 51 (1990).
[26]T. Matsushima, Surf. Sci. **127**, 403 (1983).
[27]J. E. Hurst, C. A. Becker, J. P. Cowin, K. C. Janda, L. Wharton, and D. J. Auerbach, Phys. Rev. Lett. **43**, 1175 (1979).

The Journal of Chemical Physics is copyrighted by the American Institute of Physics (AIP). Redistribution of journal material is subject to the AIP online journal license and/or AIP copyright. For more information, see http://ojps.aip.org/jcpo/jcpcr/jsp
Copyright of Journal of Chemical Physics is the property of American Institute of Physics and its content may not be copied or emailed to multiple sites or posted to a listserv without the copyright holder's express written permission. However, users may print, download, or email articles for individual use.